Available online at www.sciencedirect.com
ScienceDirect
Microelectronic Engineering 83 (2006) 2462–2468
MICROELECTRONIC ENGINEERING
www.elsevier.com/locate/mee

Assembly and reliability of PBGA packages on FR-4 PCBs with SnAgCu solder

P. Arulvanan [a], Z.W. Zhong [b,*]

[a] Singapore Institute of Manufacturing Technology, 71 Nanyang Drive, Singapore 638075, Republic of Singapore
[b] School of Mechanical and Aerospace Engineering, Nanyang Technological University, 50 Nanyang Avenue, Singapore 639798, Republic of Singapore

Received 20 February 2006; received in revised form 26 April 2006; accepted 4 May 2006
Available online 21 June 2006

Abstract

Plastic-ball-grid-array (PBGA) packages were assembled onto FR-4 printed-circuit-boards (PCBs) using lead-free SnAgCu solder, different solder pad diameters, stencil thicknesses and reflow peak temperatures, and the effects of the design and assembly process conditions on the dimensions and reliability of the solder joints were investigated. The assembled microelectronic devices were subjected to a thermal cycling test, and crack initiation and propagation during the test were studied. The results showed that with increased peak reflow temperature and pad diameter, the average joint diameter increased but the average joint height decreased. Increased stencil thickness resulted in increased joint diameters and heights. The solder joints consisted of two unique structures of Sn-rich and Ag-rich Sn–Ag compounds. The intermetallic thicknesses were less than 3 μm, and the compounds did not affect the reliability of the solder joints. Failures were not found before 5700 thermal cycles and the characteristic lives of all solder joints were more than 7200 thermal cycles, indicating robust solder joints produced with a wide process window.
© 2006 Elsevier B.V. All rights reserved.

Keywords: SnAgCu solder joints; Joint dimensions; Thermal cycling; Microstructure; Reliability

1. Introduction

Microelectronic products are used every day in our offices and home. In these products, microelectronic packaging plays important roles such as supplying power to integrated circuit (IC) chips and distributing signals among microelectronic devices. As IC fabrication advances rapidly, microelectronic packaging faces more and more challenges [1–4].

Solder joints are widely used in microelectronic packaging because they can provide mechanical and electrical connections and enhance heat spreading efficiency. The reliability of solder joints is a key issue in the design of microelectronic devices. The reliability problems are largely caused by the thermal–mechanical stresses in the solder joints associated with the temperature changes during the switch-on and -off of a microelectronic device. Predicting the reliability of solder joints is complicated [5].

Sufficient solderability of the parts used in the soldering process is a major prerequisite for the success of the process [6]. Good solderability results in good wetting, which means the formation of a uniform, smooth, unbroken, adherent coat of solder on the base metal, without the use of highly active fluxes and impairing the function of the parts soldered.

The increasing need to measure material properties of microscopic structures requires suitable techniques for strain measurements [7]. To evaluate the reliability performance of solder joints in microelectronic devices, various reliability tests are performed, which are time-consuming [8,9]. Therefore, another approach becomes popular and useful, which is to predict the fatigue life by simulating and analyzing the deformations, stresses and strains of microelectronics packages using finite element methods [10,11]. However, experimental methods are highly needed

* Corresponding author. Tel.: +65 6790 5588; fax: +65 6791 1859.
E-mail address: mzwzhong@ntu.edu.sg (Z.W. Zhong).

0167-9317/$ - see front matter © 2006 Elsevier B.V. All rights reserved.
doi:10.1016/j.mee.2006.05.002

to verify the deformations and strains obtained from the numerical simulations. One of such experimental methods is to measure deformations and strains in solder joints using a Moiré method [12,13]. Various methods to inspect solder joints have also been developed [14,15]. It has been found that interfacial preexisting voids can accelerate electromigration failures, which can reduce over a half of the solder joint lifetime with a 20% volume fraction of interfacial voids [16].

The components of the tin–lead system are completely soluble in the liquid state but only partially soluble in the solid state. This is the most common type of binary systems and is the same as for the systems of copper–silver, copper–tin, copper–zinc, aluminum–copper and aluminum–magnesium [17].

Tin–lead solders have been widely used to make microelectronic interconnections for decades. Their material properties and mathematical models for reliability prediction and the behavior of tin–lead solder joints are known readily.

With more microelectronic products required to be environmentally friendly, research on lead-free solder has become an urgent task for the microelectronic packaging industry [18]. Environmental concerns and legal constraints [19] have been pushing to replace tin–lead solders with lead-free solders or adhesives [20] in manufacturing of microelectronic devices. However, a great deal of reliability tests for lead-free solder joints are needed before they can replace traditional tin–lead solders [21]. Therefore, various lead-free alloys including binary, ternary and quaternary solders are being evaluated for use in printed circuit board (PCB) assemblies. For material and process data, lead-free solder interconnections are lacking and as such research is being conducted worldwide.

One of the most promising materials to replace tin–lead solders is SnAgCu [22]. There are three phases in the SnAgCu eutectic material, βSn and the intermetallics of Ag_3Sn and Cu_6Sn_5. The equilibrium point between Ag_3Sn and Cu_6Sn_5 is at 225 °C. The theoretical true eutectic point for the SnAgCu system lies at Sn3.4Ag0.7Cu [23].

Investigation of ball-grid-array (BGA) components with Sn3.8Ag0.7Cu alloy solder balls found an intermetallic interface of SnNiCu on NiAu PCB pads after a thermal cycling test (−55 °C to +125 °C). The solder joint failures started occurring before 2000 cycles of the thermal cycling test [24]. Lead-free solder joints have fine and stable microstructures due to formation of small-dispersed particles and consequently higher shear strengths than tin–lead solders [25]. Microstructures of Sn and plate like Ag_3Sn were observed with dendritic Sn phase for Sn3.0Ag0.5Cu alloys including Cu_6Sn_5 in SnAgCu eutectics [26]. The Ni_3Sn_4 intermetallic was found uniform and thin in Sn3.5Ag0.5Cu, while it was thick and less regular in Sn4.0Ag0.5Cu under dual reflow conditions using electroless Ni–P for BGA assemblies [27].

This work attempted to study the effects of design and assembly process conditions on lead-free SnAgCu solder joints. The process variables studied include solder pad diameters, stencil thicknesses and reflow peak temperatures. Experiments using SnAgCu solder for assembling plastic-ball-grid-array (PBGA) packages on PCBs were performed to investigate the reliability of the lead-free solder joints made under various conditions.

2. Assembly matrix and materials

Fig. 1 shows the PBGA package of 35 mm × 35 mm with 352 Sn4.0Ag0.5Cu balls assembled in this work. PCBs were designed with daisy chain loops along the outer rows of solder balls of the PBGA packages. They were fabricated with a high T_g (170 °C) FR-4 material having electroless nickel-immersion gold (NiAu) finish, and had dimensions of 150 mm × 212 mm. The daisy chains on the outer periphery of the package were routed through a PCB daisy chain designed to meet the in situ measurement requirements of the thermal-cycling chamber. The boards had a total of 12 resistance loops (one loop per package) monitored for electrical continuity during temperature cycle testing. The non-solder-mask-defined (NSMD) pads had an opening diameter of 0.66 mm on one side of the PCB and on the other side had an opening diameter of 0.56 mm. The pad sizes of 0.56 and 0.66 mm were chosen to study the effect of the variation in standoff heights on the reliability of lead-free solder joints. Before assembly, material characterization, reflow oven profiling and process validation were performed to evaluate the quality of individual components.

The PBGA packages were assembled on one side of the PCBs with Sn3.5Ag0.7Cu solder paste according to the assembly matrix shown in Table 1. Two stencils were fabricated with the same pad-opening area (0.56 mm × 0.56 mm) but different thicknesses. The paste volume on the solder pads of the PCBs was controlled

Fig. 1. Lead-free 352-ball PBGA.

Table 1
The assembly matrix and experimental results such as assembly yield, measured joint diameters and heights, and results of the thermal cycling test analyzed using the Weibull failure distribution function

Pad diameter (mm)	0.66	0.66	0.66	0.66	0.56	0.56	0.56	0.56
Stencil thickness (mm)	0.125	0.125	0.2	0.2	0.125	0.125	0.2	0.2
Reflow peak temperature (°C)	235	250	235	250	235	250	235	250
No. of PCBs	2	2	2	2	2	2	2	2
Packages assembled	24	24	24	24	24	24	24	24
Packages for micro-sectioning	6	6	6	6	6	6	6	6
Packages passed inspection	30	30	28	30	30	30	30	30
Assembly yield (%)	100	100	93	100	100	100	100	100
Average joint height (μm)	462	456	481	486	479	491	515	493
Average joint diameter (μm)	821	861	838	848	787	802	812	833
β (slope)	13.5	10.5	19.8	14.8	10.7	11	12.1	21.5
η (cycles)	7375	8085	7718	7205	7576	7780	7500	7356

using the 0.125 and 0.2 mm stencil thicknesses, representing the range typically used for mixed component PCB assemblies with fine pitch devices in manufacturing environments. The 'no-clean' solder paste used was of type-3 particle size (ANSI-J-Std-flux classification ReL0 [28]). Reflow profile conditions with peak temperatures of 235 and 250 °C were determined with the dwell time above 217 °C maintained for 90 ± 5 s. The reflow was conducted in an air environment.

3. Experimental results

3.1. Pre-assembly tests

Ten samples of the PBGA were used to perform the ball shear test specified by JEDEC Test Method B117 [29]. The average of the maximum load to shear was 13.2 N with a standard deviation of 0.7 N. The failure mode of the balls was always in the bulk solder, indicating that the interface between the ball and substrate did not exhibit any weakness.

A hot plate test similar to Test Method IPC-TM-650 [30] with reflow at a temperature 25 °C above the eutectic point (217 °C) of the solder paste was performed to study its ability to wet the surface under the specific process conditions. A schematic view of the test coupon is shown in Fig. 2. NiAu plated FR-4 PCB coupons were prepared, and solder paste was printed using a 0.2-mm-thick stencil having three ϕ6.5-mm holes. There were no significant dewetting, non-wetting, spattering and solder balling observed.

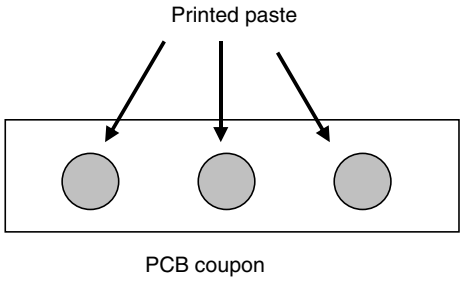

Fig. 2. A schematic view of the paste printed on the coupon.

A PCB wetting test was conducted to confirm that the PCB pad finish interacted well with the solder paste under the assembly conditions. The paste was printed on two blank PCBs using the 0.2-mm-thick matching stencil, the PCBs were reflowed, and visual inspection was conducted using an optical microscope. There were no defects such as dewetting, non-wetting and solder balling, and the wetting was uniform and good.

A package wetting test was also performed to test the package termination's interaction and wetting with the solder paste. The paste was printed on a ceramic substrate, the packages were placed, and reflow was performed using the reflow profiles. All the packages exhibited good coagulation of the solder paste with the solder ball alloy. No solder balling and other wetting related problems were observed.

3.2. Post-assembly inspections

An assembled PCB is shown in Fig. 3. Sixteen PCBs were assembled with 12 PBGA packages on each PCB following the assembly matrix (Table 1), excluding 48 additional packages for microstructure and intermetallic growth studies. The assembled PCBs were inspected under X-ray. This inspection did not find any significant defects. A typical X-ray image is shown in Fig. 4.

Out of 240 packages assembled, none of them had any open circuit after assembly except two. The detailed assembly yield breakdown is shown in Table 1.

The dimensions (diameter D and height H shown in Fig. 5) of four solder joints in each category were measured during scanning electron microscopy (SEM) analysis, and the average dimensions are shown in Table 1. Table 2 shows the effects of the peak reflow temperature, stencil thickness and pad diameter on the average diameters and heights of the solder joints. Increased stencil thickness resulted in increased solder paste volume and therefore increased joint diameters and heights. With increased peak reflow temperature and pad diameter, the average joint diameter increased but the average joint height decreased.

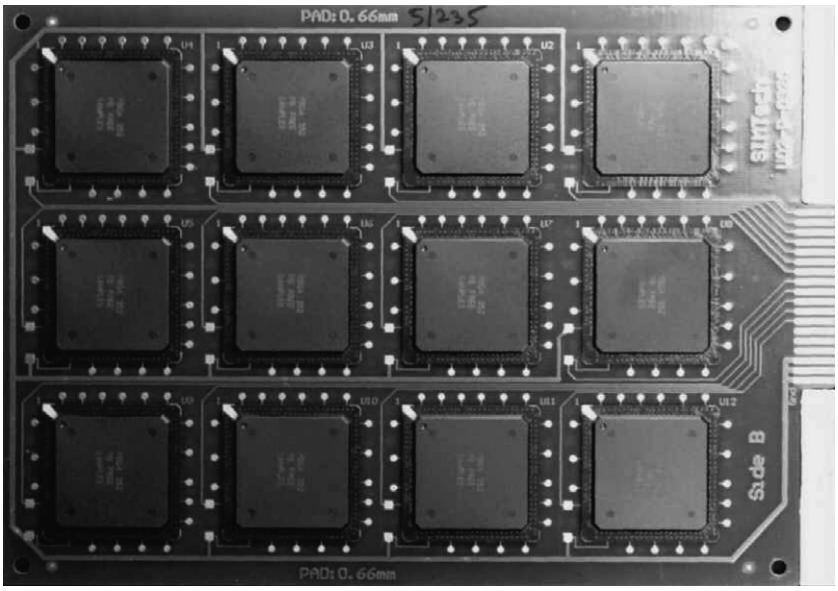

Fig. 3. An assembled PCB with 12 PBGA packages.

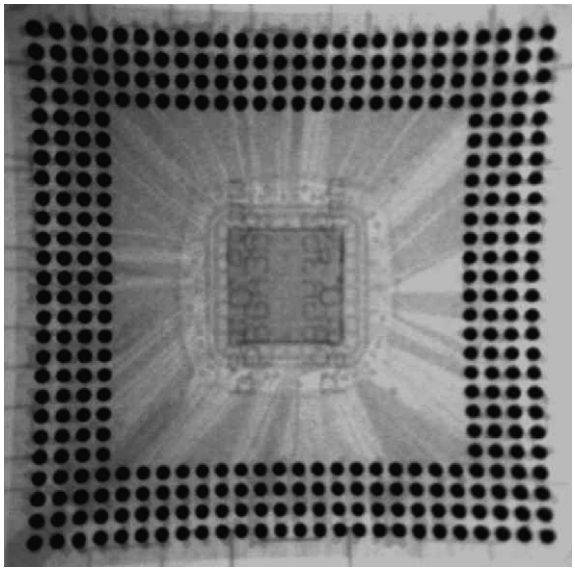

Fig. 4. A typical X-ray image showing no solder bridging defects.

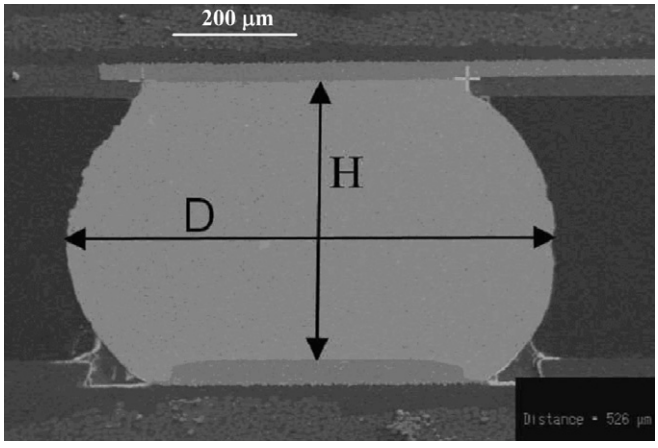

Fig. 5. Measurements of solder dimensions (diameter D and height H).

Table 2
The average solder-joint heights and diameters

Factor	Value	Average diameter (μm)	Average height (μm)
Reflow peak temperature (°C)	235	815	484
	250	836	482
Stencil thickness (mm)	0.125	818	472
	0.2	833	494
Pad diameter (mm)	0.56	809	495
	0.66	842	471

3.3. Thermal cycling test and failure analysis

A temperature cycling test (−40/+125 °C) was conducted with a ramp rate of 10–14 °C/min and 15 min of dwell time. The daisy chain resistance of all the tested assemblies was continuously monitored by a data acquisition system at the temperature extremes of each cycle. The failure criterion adopted was a verified resistance increase of more than 300 Ω from the initial measurement for any test loop. All of the tested packages passed the thermal cycling test successfully up to 5700 cycles. The test was continued and the collected failure data was analyzed using the Weibull failure distribution function as shown in Table 1. The characteristic life to 63% failure of all the packages tested was above 7200 thermal cycles, indicating reliable lead-free solder joints could be made over a wide process window allowing flexibility in design and manufacturing in mass production environments.

Thermal cycled samples were removed from the testing chamber after 500, 1000, 2000 and 3000 cycles. Microsec-

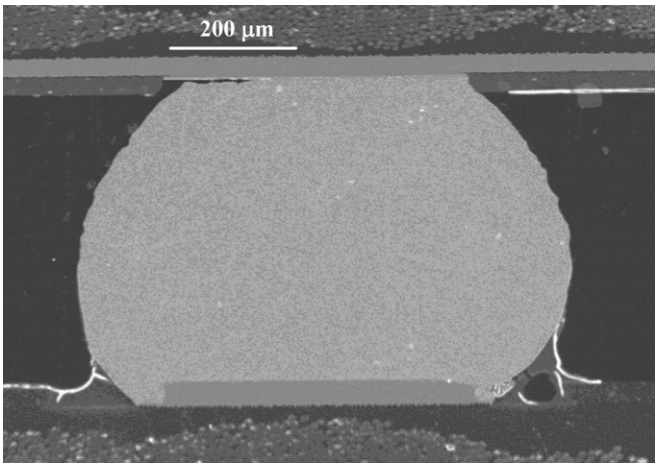

Fig. 6. Crack propagation after 2000 thermal cycles (0.2-mm stencil thickness, 250 °C reflow, 0.66-mm pad).

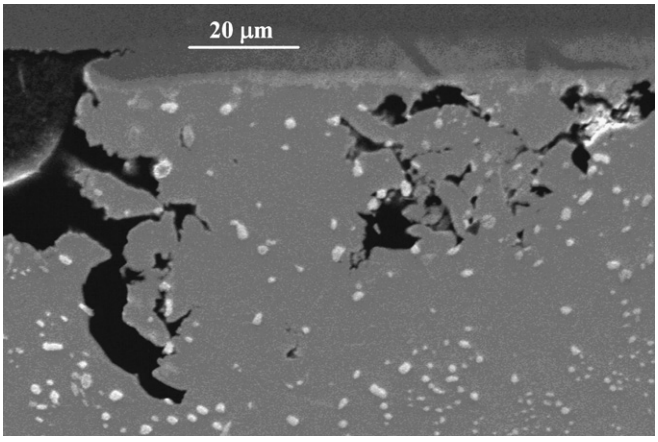

Fig. 7. Crack propagation/spalling after 2000 thermal cycles (0.125-mm stencil thickness, 235 °C reflow, 0.66-mm pad).

tions of these samples were analyzed to study the crack initiation and growth mechanism. Although there was no electrical failure in the daisy chain loops before 5700 thermal cycles, potential failure modes of solder joints could be seen from the microsections after certain thermal cycles. No crack initiation was observed after 500 thermal cycles, but crack initiation was obvious after 1000 thermal cycles.

Figs. 6 and 7 show crack propagation/spalling after 2000 thermal cycles. Cracks originated at one of the solder-joint corners at the package solder-mask-defined-pad side. These corners had a high strain compared to the PCB side with NSMD pads. Solder extended along the periphery of the NSMD pads at the PCB side, forming a more robust structure.

The spalling of solder joints was observed only at certain locations in the samples immediately after 2000 thermal cycles, but was predominant in the samples after 3000 cycles. The reflow peak temperatures did not cause any significant changes in failure modes. The variations in pad size and solder paste volume did not affect solder joint failures significantly either. The effect of pad size combined with solder paste volume, leading to a variation of 5% in solder joint height, did not result in distinguishable variations in failures. SnAgCu solder joints could be produced with a wide process window without any significantly bad effect on the product reliability.

3.4. Investigation of microstructure and intermetallic growth

Investigation of microstructure and intermetallic growth of the solder joints was conducted using SEM and energy dispersive spectroscopy (EDS) techniques after various cycles of the thermal cycling test.

Fig. 8 shows a typical microstructure of the solder joints. Small worm-shaped Sn-rich Sn–Ag (type-1) compounds existed in abundance along grain boundaries of the Sn matrix. Electroless-nickel-immersion-gold (ENIG) surface finish on both substrate and PCB pads resulted in intermetallic interface layers of Sn–Ni–Cu at both ends of a solder joint. The thicknesses of the intermetallic interface layers at the PCB and substrate sides had averages of 2.3 and 2.7 μm, respectively.

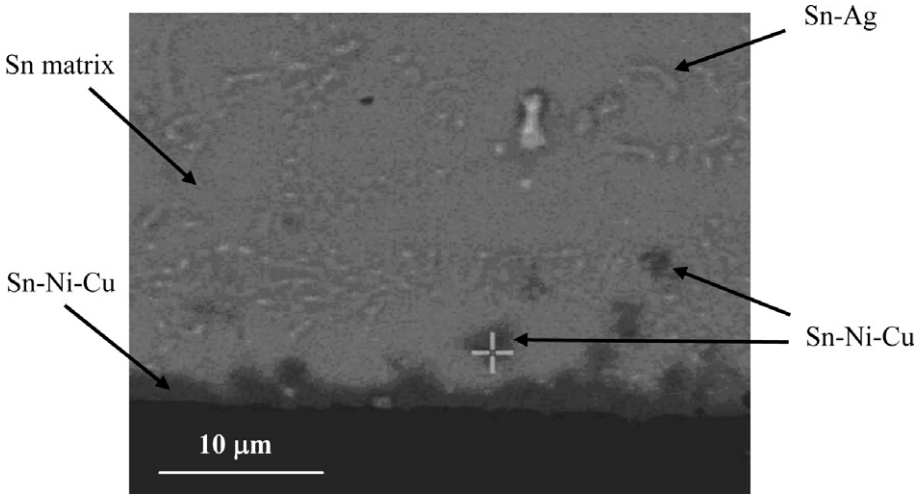

Fig. 8. Example of solder joint microstructure at the PCB-side interface.

Big crystalline rod-shaped Ag-rich Sn–Ag (type-2) compounds also existed extending across many grains at random locations, as shown in Fig. 9. The type-1 compound existed uniformly across the whole solder joint along grain boundaries, while the type-2 compound was not commonly found in all solder joints. A star-shaped P–Sn–Ni–Cu structure was found in one solder joint after 3000 thermal cycles (Fig. 10).

SEM images of the solder joints were also used to measure the intermetallic thickness with the aid of an image analyzer. Measurements were performed at three different locations for each category of the conditions in Table 1, and an average was derived over a range of thermal cycles (0–3000 cycles). The microstructures at the interface of the PBGA substrate pad and solder joint were found to be the same as those at the interface of the PCB pad side, containing Sn–Ni–Cu intermetallics, 2–3 μm thick in all of the solder joints investigated. The intermetallic growth at both the PCB and substrate sides after 3000 thermal cycles was less than 10%. Fig. 11 shows an SEM image of the interface at the PCB side after 3000 thermal cycles.

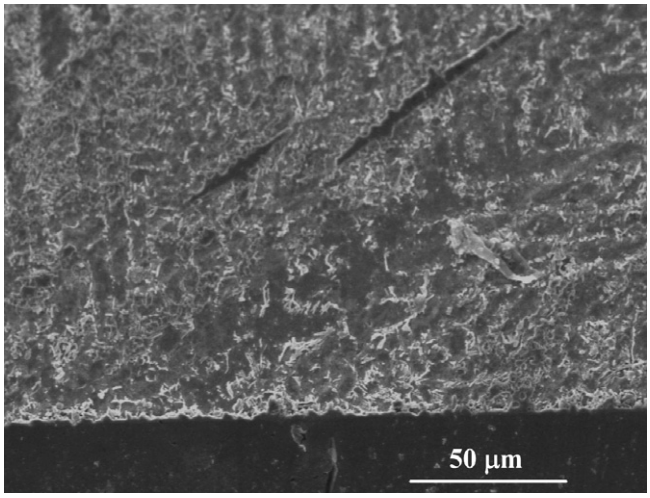

Fig. 9. Sn–Ag type-2 intermetallic compound in a solder joint.

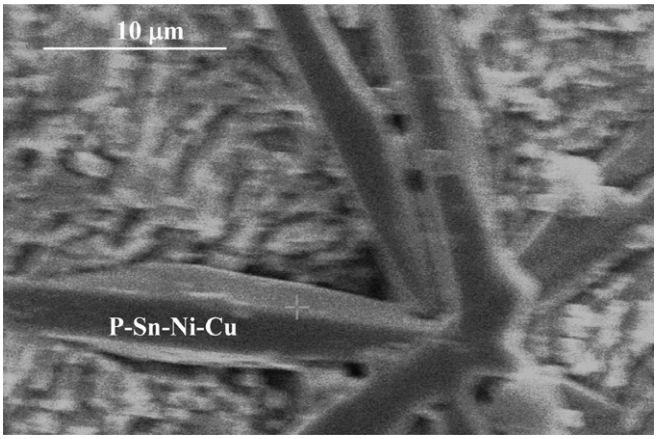

Fig. 10. A star-shaped P–Sn–Ni–Cu structure (after 3000 thermal cycles).

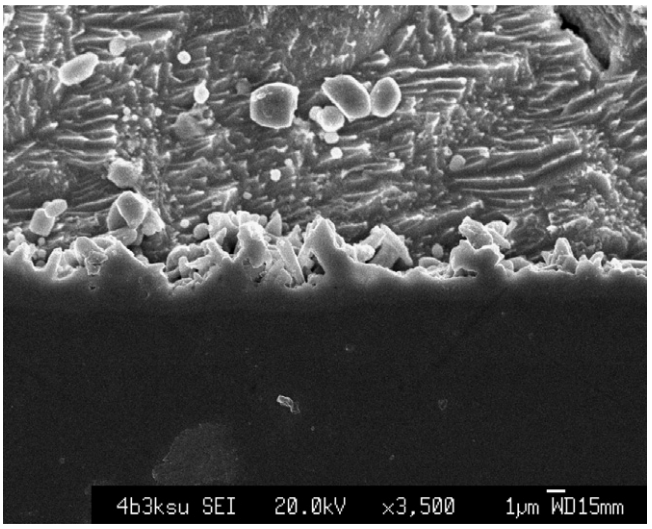

Fig. 11. The solder joint interface at the PCB side after 3000 thermal cycles.

3.5. Comparison with previous studies

The Sn–Ag type-1 structure was found in both Ref. [31] and this work. Another precipitate of Cu_6Sn_5 having a hexagonal crystal structure with a grain size of 0.3 μm mainly distributed in the Sn matrix, and finely dispersed voids along the intermetallic layer were found in Ref. [31] but not in this work. In their study the solder was heated up to 280 °C before it was cooled down to the room temperature, while in our study PCBs were reflowed at not more than 250 °C.

The Ag–Sn type-2 structure found in our study can be confirmed to be the same as the Ag_3Sn plates reported in Ref. [32]. In-line with our findings, small secondary cracks and spalling of solder were also observed. A phosphorous-rich layer was found on all ENIG plated surfaces, and Ni/Au finish produced numerous small voids around the intermetallic formation [32], which were not encountered in our study. The intermetallic compounds at the interfaces consisting of Cu–Sn [33] and the Cu–Au–Ni–Sn compound [34] were not present in the samples of this work. The failure mechanisms in our study are in concurrence with the conclusion drawn in Ref. [35].

4. Conclusions

With increased peak reflow temperature and pad diameter, the average joint diameter increased but the average joint height decreased. Increased stencil thickness resulted in increased joint diameters and heights. Crack initiation and propagation occurred along the interface between the bulk solder and the intermetallic layer in the bulk solder side. The solder joints consisted of two unique structures of Sn-rich and Ag-rich Sn–Ag compounds. A crystalline star-shaped structure of Sn–Ni–Cu–P was also observed in a solder joint. The intermetallic thicknesses were less than 3 μm. The compounds did not affect the reliability

of solder joints. No failures of the daisy chain resistance loops were reported up to 5700 thermal cycles. The characteristic lives of all solder joints produced using different process and design parameters were more than 7200 thermal cycles, indicating robust solder joints produced with a wide process window. Findings were compared with those in previous studies, and the comparison proved the validity of this work. The findings provide great confidence to implement a lead-free soldering process without compromising reliability.

Acknowledgement

The authors thank Dr. X.Q. Shi of SIMTech for his cooperation.

References

[1] Z. Zhong, Microelectronics International 16 (3) (1999) 6–14.
[2] P. Palm, J. Maattanen, A. Picault, Y. De Maquille, Microelectronics International 18 (3) (2001) 27–31.
[3] Z. Zhong, Microelectronics International 17 (2) (2000) 15–18.
[4] C.P. Wong, S. Luo, Z. Zhang, Science 290 (5500) (2000) 2269–2270.
[5] Q.D. Yang, D.J. Shim, S.M. Spearing, Microelectronic Engineering 75 (1) (2004) 85–95.
[6] R.J.K. Wassink, Soldering in Electronics: A Comprehensive Treatise on Soldering Technology for Surface Mounting and Through-Hole Techniques, Electrochemical Publications, Scotland, 1989.
[7] D. Vogel, R. Kuhnert, M. Dost, B. Michel, Journal of Electronic Packaging 124 (2002) 345–351.
[8] Z. Zhong, Soldering & Surface Mount Technology 13 (2) (2001) 21–25.
[9] C.Y. Huang, Microelectronics International 21 (2) (2004) 10–15.
[10] Z. Zhong, P.K. Yip, Soldering & Surface Mount Technology 15 (1) (2003) 21–25.
[11] J. Mackerle, Modelling and Simulation in Materials Science and Engineering 10 (2002) 637–671.
[12] Z.W. Zhong, S.K. Nah, Soldering & Surface Mount Technology 15 (3) (2003) 33–35.
[13] Z.W. Zhong, Microelectronics International 21 (3) (2004) 25–28.
[14] Y.G. Lu, L.Z. Jiang, L.X. Zou, W.Z. Geng, J. Hong, NDT & E International 23 (3) (1990) 157–160.
[15] S.T. Kang, H.S. Cho, NDT & E International 32 (1) (1999) 9–20.
[16] Z. Tang, F.G. Shi, Microelectronics Journal 32 (7) (2001) 605–613.
[17] H.H. Manko, Solders and Soldering, Materials, Design, Production, and Analysis for Reliable Bonding, McGraw-Hill, New York, NY, 2001.
[18] K.C. Chan, Z.W. Zhong, K.W. Ong, Soldering & Surface Mount Technology 15 (2) (2003) 46–52.
[19] M. Bigas, E. Cabruja, Microelectronics Journal 37 (4) (2006) 308–316.
[20] P. Palm, J. Maattanen, Y. De Maquille, A. Picault, J. Vanfleteren, B. Vandecasteele, Microelectronics Reliability 43 (2003) 445–451.
[21] J.-M. Koo, S.-B. Jung, Microelectronic Engineering 82 (3–4) (2005) 569–574.
[22] J. Helneder, C. Hoyler, M. Schneegans, H. Torwesten, Microelectronic Engineering 82 (3–4) (2005) 581–586.
[23] NIST, National Institute of Standards and Technology database, Phase Diagrams & Computational Thermodynamics. <http://www.metallurgy.nist.gov/phase/solder/agcusn.html>, 2004 (accessed 12.09.04).
[24] A. Anand, Y.C. Mui, in: Proceedings of the 4th IEEE Electronic Packaging Technology Conference, Singapore, 2002, p. 6–10.
[25] L.L. Ye, Z. Lai, J. Liu, A. Tholen, in: Proceedings of the 50th IEEE Electronic Components and Technology Conference, Las Vegas, USA, 2000, p. 134–137.
[26] Y. Mutoh, J. Zhao, Y. Miyashita, C. Kanchanomai, Soldering & Surface Mount Technology 14 (3) (2002) 37–45.
[27] G.R. Minogue, in: Proceedings of the Technical Conference of IPC Printed Circuits Expo (APEX 2002), San Diego, CA, 2002, S06 3.1–3.6.
[28] IPC/EIA, Requirements for Soldering Fluxes, IPC/EIA J-STD-004A, EIA, Arlington, VA and IPC, Northbrook, IL, 1996.
[29] JEDEC Solid State Technology Association, JEDEC Standard BGA Ball Shear, JESD22-B117, EIA, Arlington, VA, 2000.
[30] IPC, IPC-TM-650 Test Methods Manual, IPC/EIA J-STD-004A, IPC, Northbrook, IL, 1995.
[31] L. Ye, Z.H. Lai, J. Liu, A. Tholen, Soldering and Surface Mount Technology 13 (3) (2001) 6–20.
[32] S.O. Dunford, A. Primavera, M. Meilunas, Microstructural evolution and damage mechanisms in Pb-free solder joints during extended −40 °C to 125 °C thermal cycles, Technical article, IPC Review Magazines, December 2002, 8–9, and January 2003, 10–11.
[33] P. Roubaud, G. Ng, G. Henshall, R. Bulwith, R. Herber, S. Prasad, in: Proceedings of the Technical Conference of IPC Printed Circuits Expo (APEX 2002), San Diego, CA, 2002, LF2-3.
[34] L.C. Shiau, C.E. Ho, C.R. Kao, Soldering & Surface Mount Technology 14 (3) (2002) 25–29.
[35] F.A. Stam, E. Davitt, Microelectronics Reliability 41 (2001) 1815–1822.